SUPPORTING INFORMATION

Metabolism of a Bioorthogonal PET Tracer Candidate [^{19}F/^{18}F]SiFA-Tetrazine in Mouse Liver Microsomes: Biotransformation Pathways and Defluorination Investigated by UHPLC-HRMS

Sofia Otaru[†], Hanna Niemikoski[‡], Mirkka Sarparanta[†], Anu J. Airaksinen[†,§]**

[†]Radiochemistry, Department of Chemistry, University of Helsinki, Finland

[‡]Finnish Institute for Verification of the Chemical Weapons Convention (VERIFIN), Department of Chemistry, University of Helsinki, Finland

[§]Turku PET Centre, Department of Chemistry, University of Turku, 20500 Turku, Finland

*Corresponding author: Sofia Otaru and Anu Airaksinen

Radiochemistry, Department of Chemistry P.O. Box 55, FI-00014 University of Helsinki, Finland. E-mail: sofia.otaru@helsinki.fi, anu.airaksinen@helsinki.fi

Keywords: *defluorination; metabolism; positron emission tomography; silicon fluoride acceptor; tetrazine; geometric isomers*

Table of contents

Biodistribution of [^{18}F]SiFA-Tz and *in vivo* defluorination.

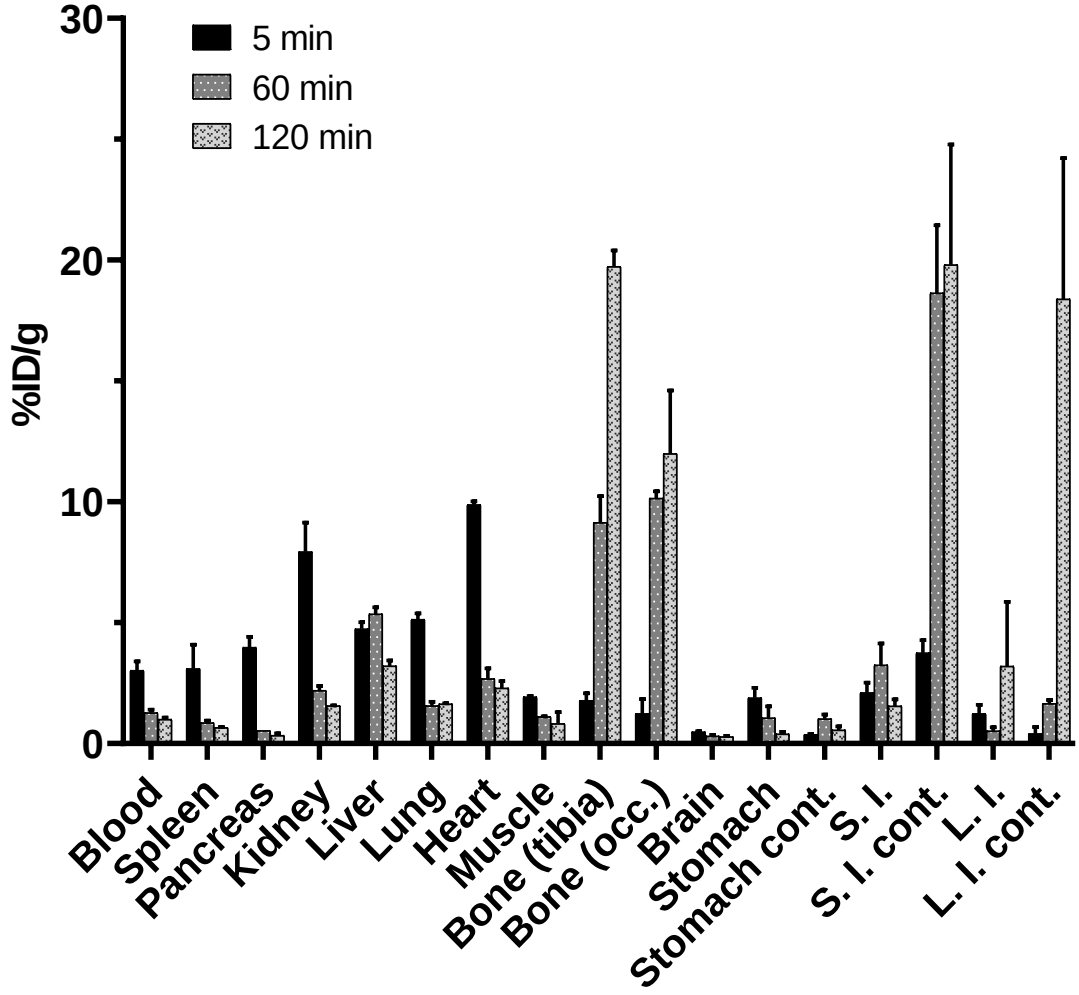

Figure S1. The biodistribution of [^{18}F]**SiFA-Tz** (t = 5, 60 and 120 min., n = 2) in healthy CD-1 mice demonstrated rapid clearance from the blood stream, but a rapid and high bone uptake 60 minutes post-injection, attributed presumably to fast metabolism leading to *in vivo* defluorination, was also detected (occ., occipital; S.I, small intestines; L.I, large intestines). The administered dose was 8.8 ± 0.3 MBq (53.1 ± 0.9 nmol, n = 6) of [^{18}F]**SiFA-Tz**.

Table S1. Conditions used for generating *in vitro* metabolites in MLMs.

Sample	*SiFA–Tz*	*NADPH*	*UDPGA*	*MLM*	*Alamethicin*	**Buffer*	*Time (min)*
Phase I	✓	✓		✓		✓	5, 60, 120, 240
Phase II	✓	✓	✓	✓	✓	✓	5, 60, 120, 240
Control 1	✓	✓	✓	✓	✓	✓	0
Control 2		✓		✓	✓	✓	0
Control 3	✓		✓	✓	✓	✓	5, 60, 120, 240
Control 4	✓	✓	✓		✓	✓	5, 60, 120, 240

*Buffer = 100 mM Potassium phosphate solution pH 7.4.

MS/HRMS spectrum, mass differences and proposed fragments of SiFA-Tz.

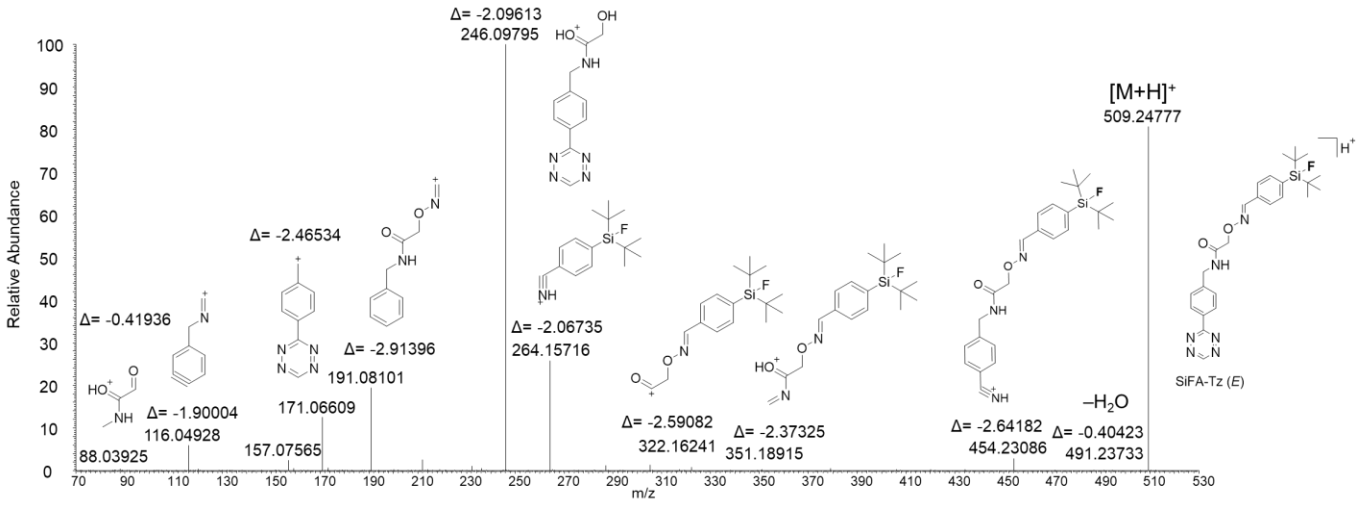

Figure S2. The MS/HRMS-spectrum and proposed fragmentation pattern of **1** (*E*-isomer) with assigned proposed possible fragments using HCD 30% (Δ; mass difference in ppm).

MS/HRMS spectrum, mass differences and proposed fragments of SiFA−H_2Tz.

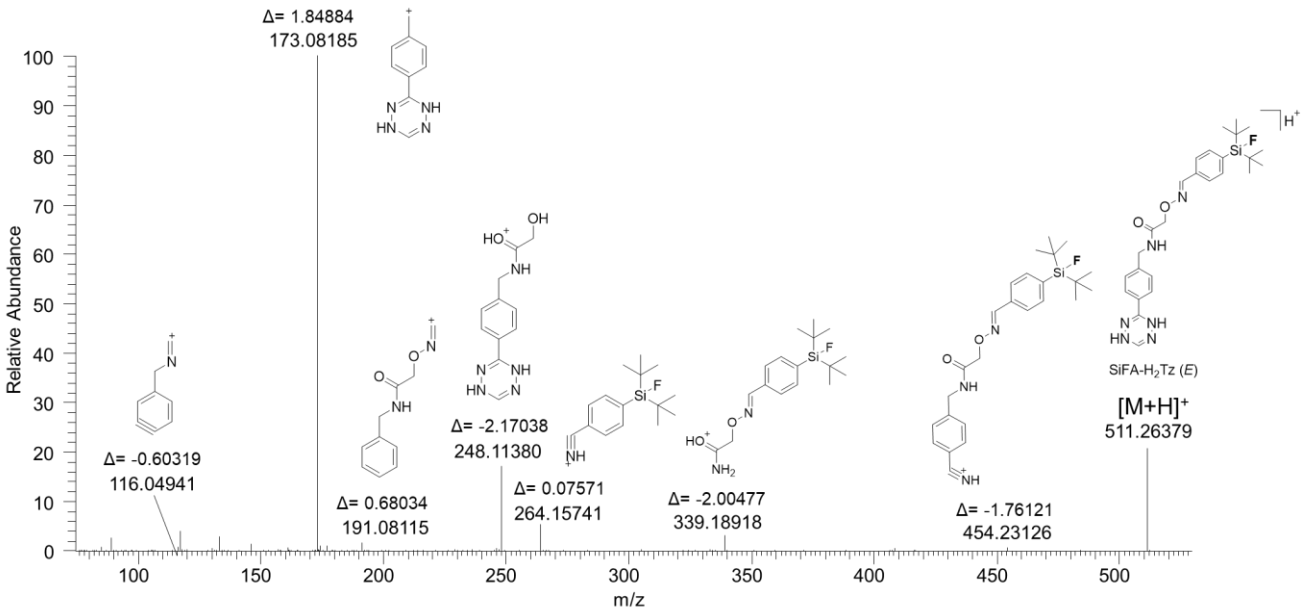

Figure S3. The MS/HRMS-spectrum and proposed fragmentation pattern of **(*E*)-SiFA-H_2Tz** with assigned proposed fragments using HCD 25%. Diagnostic fragments at *m/z* 173 and at *m/z* 248 indicate reduction of the tetrazine ring (Δ; mass difference in ppm).

Relative abundances of *E*- and *Z*-isomers of SiFA−Tz and SiFA−H_2Tz in analytical standard, control and *in vitro* samples.

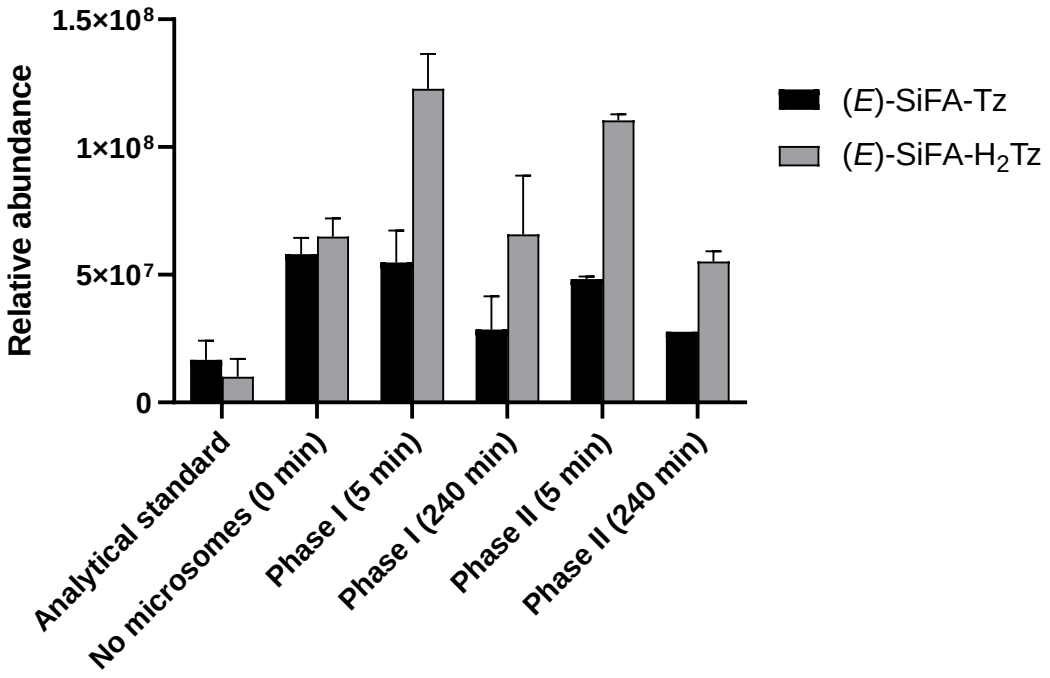

Figure S4. Relative abundances of *E*- and *Z*-isomers of **SiFA−Tz and SiFA−H_2Tz** in analytical standard, control and *in vitro* samples.

Relative abundances of *E*- and *Z*-isomers of SiFA-Tz in standard sample.

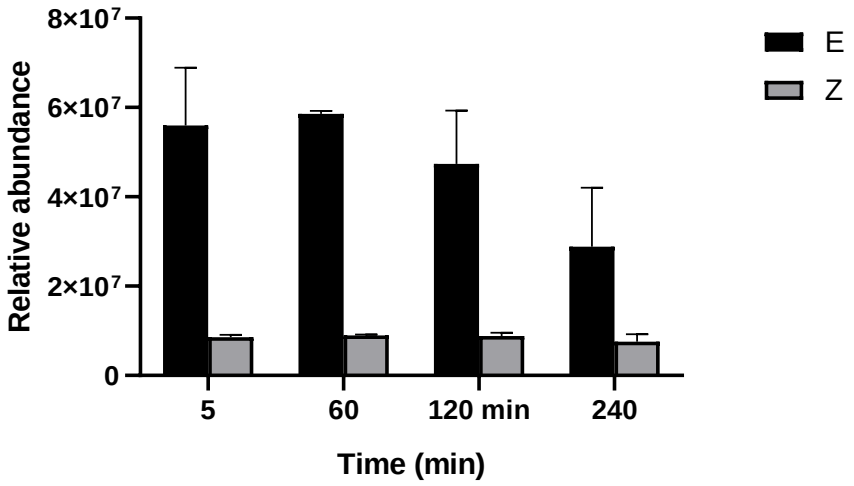

Figure S5. Difference in metabolism speed of isomers.

Table S2. Elemental compositions, theoretical masses, measured masses, mass differences, proposed structures and retention times of proposed phase I metabolites of SiFA–Tz.

Compd.	Formula $[M + H]^+$	Theoretical mass (*m/z*)	Observed mass (*m/z*)	Mass difference (ppm)	Proposed structure	T_R (min)
SiFA—Tz	$C_{26}H_{34}FN_6O_2Si^+$	509.24911	509.24905 (*E*) 509.24900 (*Z*)	0.01860 (*E*) -0.20865 (*Z*)	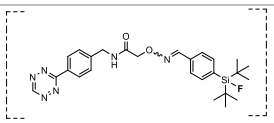	4.64 4.37
M1	$C_{26}H_{34}FN_6O_3Si^+$	525.24402	525.24329 (*E*)	-1.39742	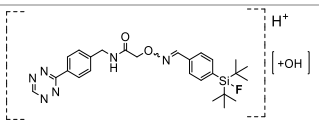	3.68
M2	$C_{26}H_{34}FN_6O_3Si^+$	525.24402	525.24323	-1.51363	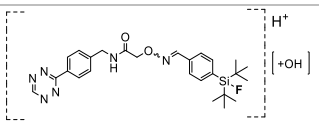	3.64
M3	$C_{26}H_{35}N_6O_4Si^+$	523.24836	523.24753	-1.57599	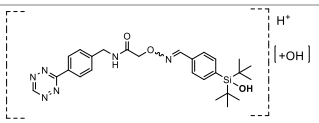	2.58
M4	$C_{26}H_{35}N_6O_5Si^+$	539.24327	539.24237	-1.67413	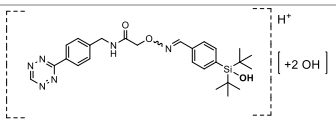	2.55
M5	$C_{26}H_{35}N_6O_5Si^+$	539.24327	539.24240	-1.61091	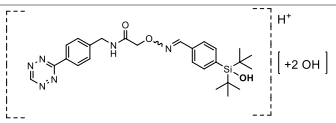	2.27

Table S3. Elemental compositions, theoretical masses, measured masses, mass differences, proposed structures and retention times of proposed phase I metabolites of SiFA–H_2Tz.

Compd.	Formula $[M + H]^+$	Theoretical mass (*m/z*)	Observed mass (*m/z*)	Mass difference (ppm)	Proposed structure	T_R (min)
SiFA–H_2Tz	$C_{26}H_{36}FN_6O_2Si^+$	511.26476	511.26478 (*E*) 511.26478 (*Z*)	0.04872 (*E*) 0.04429 (*Z*)	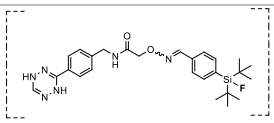	4.37 / 4.24
M(H_2)1	$C_{26}H_{36}FN_6O_3Si^+$	527.25967	527.25877	-1.70607	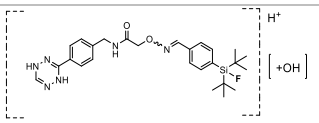	3.86
M(H_2)2	$C_{26}H_{36}FN_6O_3Si^+$	527.25967	527.25873	-1.77457	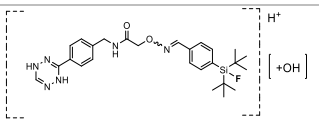	3.63
M(H_2)3	$C_{26}H_{37}N_6O_4Si^+$	525.26401	525.26303	-1.85681	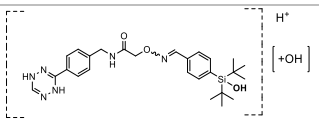	2.83
M(H_2)4	$C_{26}H_{37}N_6O_4Si^+$	525.26401	525.26305	-1.82880	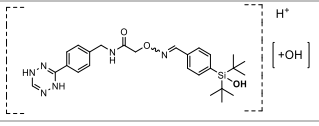	2.53

Formation of defluorinated metabolite of SiFA–H_2Tz as its proposed geometric *E*- (M(H_2)3) and *Z*-isomers (M(H_2)4) incubated in mouse liver microsomes.

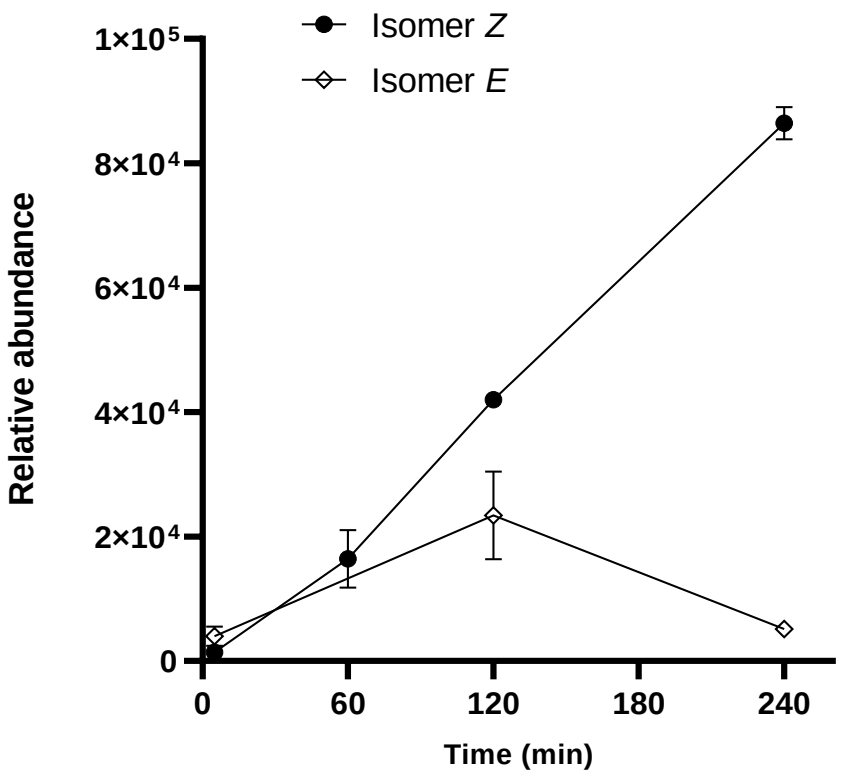

Figure S6. The formation of defluorinated metabolite of SiFA–H_2Tz as its proposed geometric *E*-(**M(H_2)3**) and *Z*-isomers (**M(H_2)4**) (*m/z* 525.26401) incubated in mouse liver microsomes. The difference in peak areas indicated the *E*-isomer was metabolized further and the *Z*-isomer was more resistant to further biotransformation.

Table S4. Elemental compositions, theoretical masses, measured masses, mass differences, proposed structures and retention times of proposed phase II metabolites of SiFA–Tz.

Compd.	Formula $[M + H]^+$	Theoretical mass (*m/z*)	Observed mass (*m/z*)	Mass difference (ppm)	Proposed structure	T_R (min)
SiFA—Tz	$C_{26}H_{34}FN_6O_2Si^+$	509.24911	509.24905 (*E*) 509.24900 (*Z*)	0.01860 (*E*) -0.20865 (*Z*)	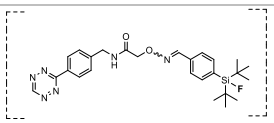	4.64 4.37
M6	$C_{32}H_{42}FN_6O_9Si^+$	701.27611	701.27497	-1.62253	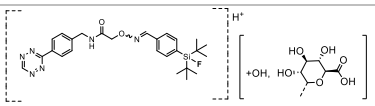	3.67
M7	$C_{32}H_{42}FN_6O_9Si^+$	701.27611	701.27492	-1.69332	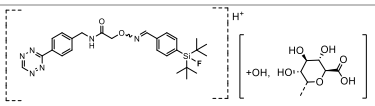	3.64
M8	$C_{32}H_{43}N_6O_{10}Si^+$	699.28044	699.28054	0.13626	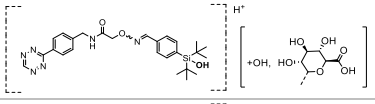	2.96
M9	$C_{32}H_{43}N_6O_{10}Si^+$	699.28044	699.28039	-0.07358	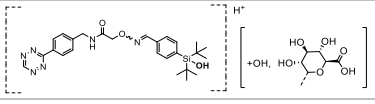	2.89

Table S5. Elemental compositions, theoretical masses, measured masses, mass differences, proposed structures and retention times of proposed phase II metabolites of SiFA–H_2Tz.

Compd.	Formula $[M + H]^+$	Theoretical mass (*m/z*)	Observed mass (*m/z*)	Mass difference (ppm)	Proposed structure	T_R (min)
SiFA–H_2Tz	$C_{26}H_{36}FN_6O_2Si^+$	511.26476	511.26478 (*E*) 511.26478 (*Z*)	0.04872 (*E*) 0.04429 (*Z*)	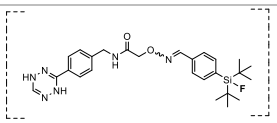	4.37 / 4.24
M(H_2)5	$C_{32}H_{44}FN_6O_9Si^+$	703.29176	703.29099	-1.08514	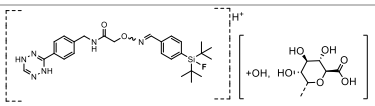	2.73
M(H_2)6	$C_{32}H_{44}FN_6O_9Si^+$	703.29176	703.29058	-1.68090	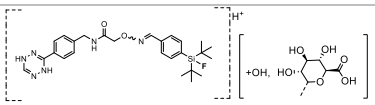	2.50
M(H_2)7	$C_{32}H_{45}N_6O_{10}Si^+$	701.29609	701.29471	-1.97998	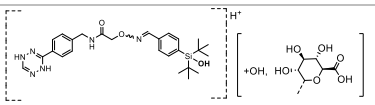	2.34
M(H_2)8	$C_{32}H_{45}N_6O_{10}Si^+$	701.29609	701.29540	-0.98842	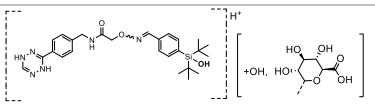	2.20

Formation of *o*-glucuronide conjugate metabolites M6 and M8 in MLMs.

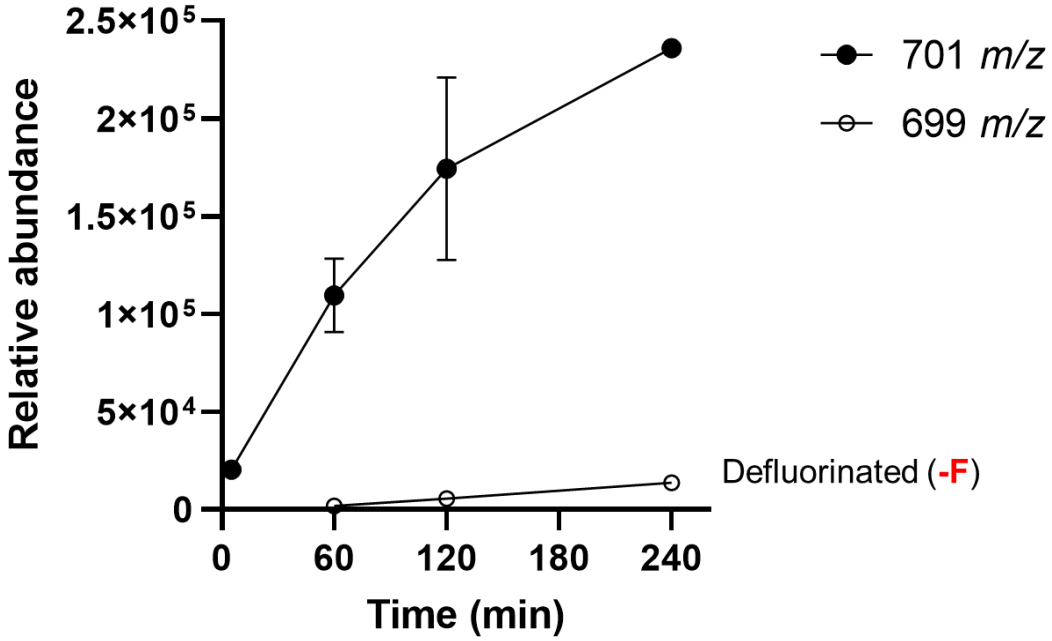

Figure S7. Formation of *o*-glucuronide conjugate metabolites **M6** (*m/z* 701) and defluorinated **M8** (*m/z* 699) of SiFA–H_2Tz in mouse liver microsomes.

Formation of proposed *o*-glucuronide conjugate metabolites M(H$_2$)5 and defluorinated M(H$_2$)7.

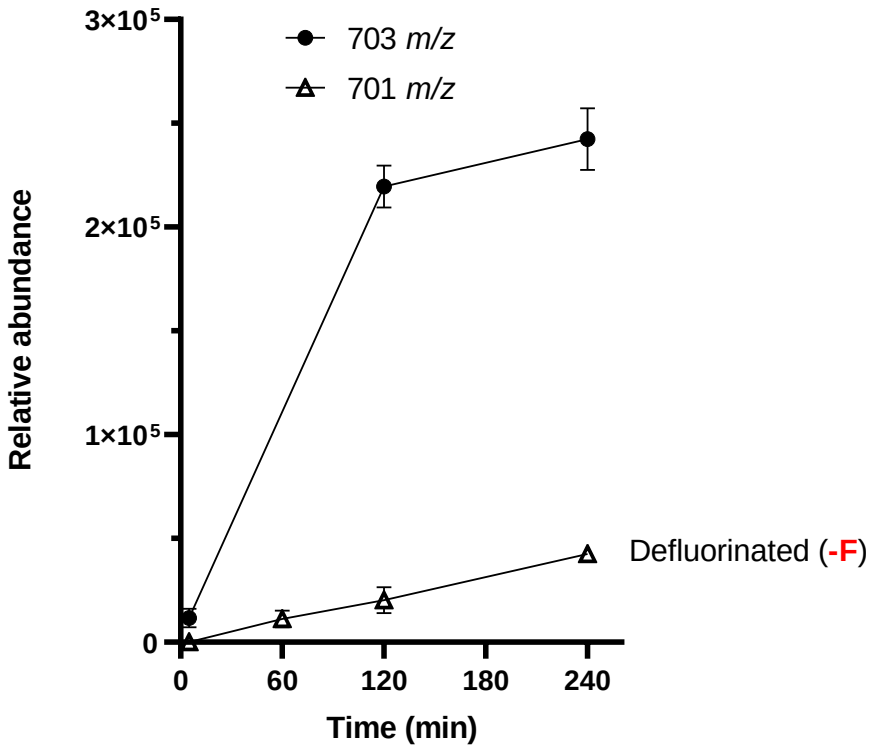

Figure S8. Formation of *o*-glucuronide conjugate metabolites **M(H$_2$)5** (*m/z* 703) and defluorinated **M(H$_2$)7** (*m/z* 701) of SiFA–H$_2$Tz in mouse liver microsomes.

Table S6. Theoretical masses, retention times, biotransformations and major fragments of proposed metabolites of SiFA–Tz and SiFA-H_2Tz detected in *in vitro* samples.

Compd. ID	T_R	Biotransformation	Observed mass (*m/z*)	Ms^n fragments (*m/z*)
(*E*)-SiFA–Tz	4.64	(Parent)	509.24905	491.23733, 454.23086, 351.18915, 322.16241, 264.15716 (75%), 246.09795 (93%), 191.08101, 171.06609, 116.04928, 88.03925
(*Z*)-SiFA–Tz	4.37	(Parent)	509..24900	454.23352, 351.19031, 264.15821 (63%), 246.09920 (79%), 191.08200, 171.06696, 116.04928
M1	3.68	Hydroxylation	525.24329	451.17084, 396.15384, 354.10693, 246.09856, 191.08153, 171.06651
M2	3.64	Hydroxylation	525.24323	451.17072, 396.15369, 246.09857, 191.08159, 116.04955
M3	2.58	Hydroxylation	523.24753	505.35385, 451.19080, 421.18030, 378.17447, 173.08218
M4	2.55	Dihydroxylation, oxidative defluorination	539.24237	507.76541, 489.86511, 389.63953, 245.94293, 173.09607
M5	2.27	Dihydroxylation, oxidative defluorination	539.24240	521.24384, 448.38474, 418.03268, 332.88428, 353.26602, 263.93127, 191.16951, 173.04382
M6	3.67	Hydroxylation, *o*-glucuronidation	701.27497	451.16956, 396.15280, 354.10587, 246.09789, 191.08148, 171.06653, 116.04959
M7	3.64	Hydroxylation, *o*-glucuronidation	701.27492	471.72101, 396.15372, 354.19681, 246.09866, 171.06660, 116.04957
M8	2.96	Hydroxylation, oxidative defluorination, *o*-glucuronidation	699.28054	505.63568, 487.14490, 449.18030, 394.15790, 376.14758
M9	2.89	Hydroxylation, oxidative defluorination, *o*-glucuronidation	699.28039	505.24277, 449.18033, 394.15805, 376.16394
(*E*)-SiFA–H_2Tz	4.36	(Parent)	511.26478	454.23126, 339.18918, 334.19772, 264.15741, 248.11380, 191.08115, 173.08185, 116.054941
(*Z*)-SiFA–H_2Tz	4.24	(Parent)	511.26478	334.19742, 264.15717, 248.11362, 173.08174
M(H_2)1	3.86	Hydroxylation	527.25877	509.24899, 453.18646, 424.17252, 396.15378, 351.15625, 248.11424, 173.08220, 118.06523
M(H_2)2	3.63	Hydroxylation	527.25873	509.24936, 453.18643, 423.17606, 380.17004, 248.84013
M(H_2)3	2.83	Hydroxylation, oxidative defluorination	525.26303	451.19073, 422.17967, 394.15814, 323.15738, 173.08214
M(H_2)4	2.53	Hydroxylation, oxidative defluorination	525.26305	507.36029, 451.19086, 421.18027, 378.17444, 351.16339, 248.11417, 173.08214
M(H_2)5	2.73	Hydroxylation, *o*-glucuronidation	703.29099	527.25964, 509.24911, 453.18649, 424.17252, 396.15381, 248.11435, 173.08217, 118.06525
M(H_2)6	2.50	Hydroxylation, *o*-glucuronidation	703.29058	527.25909, 509.24902, 453.18649, 423.17590, 396.27402, 380.17004, 173.08212
M(H_2)7	2.34	Hydroxylation, oxidative defluorination, *o*-glucuronidation	701.29471	525.24188, 507.23177, 451.16901, 396.15213, 394.15677, 352.11020, 248.49008, 173.08167
M(H_2)8	2.20	Hydroxylation, oxidative defluorination, *o*-glucuronidation	701.29540	525.24243, 507.23135, 451.16916, 396.15231, 349.13953, 248.11385, 173.08191

MS/HRMS spectrum and fragments of proposed phase I and phase II metabolites of SiFA-H$_2$Tz.

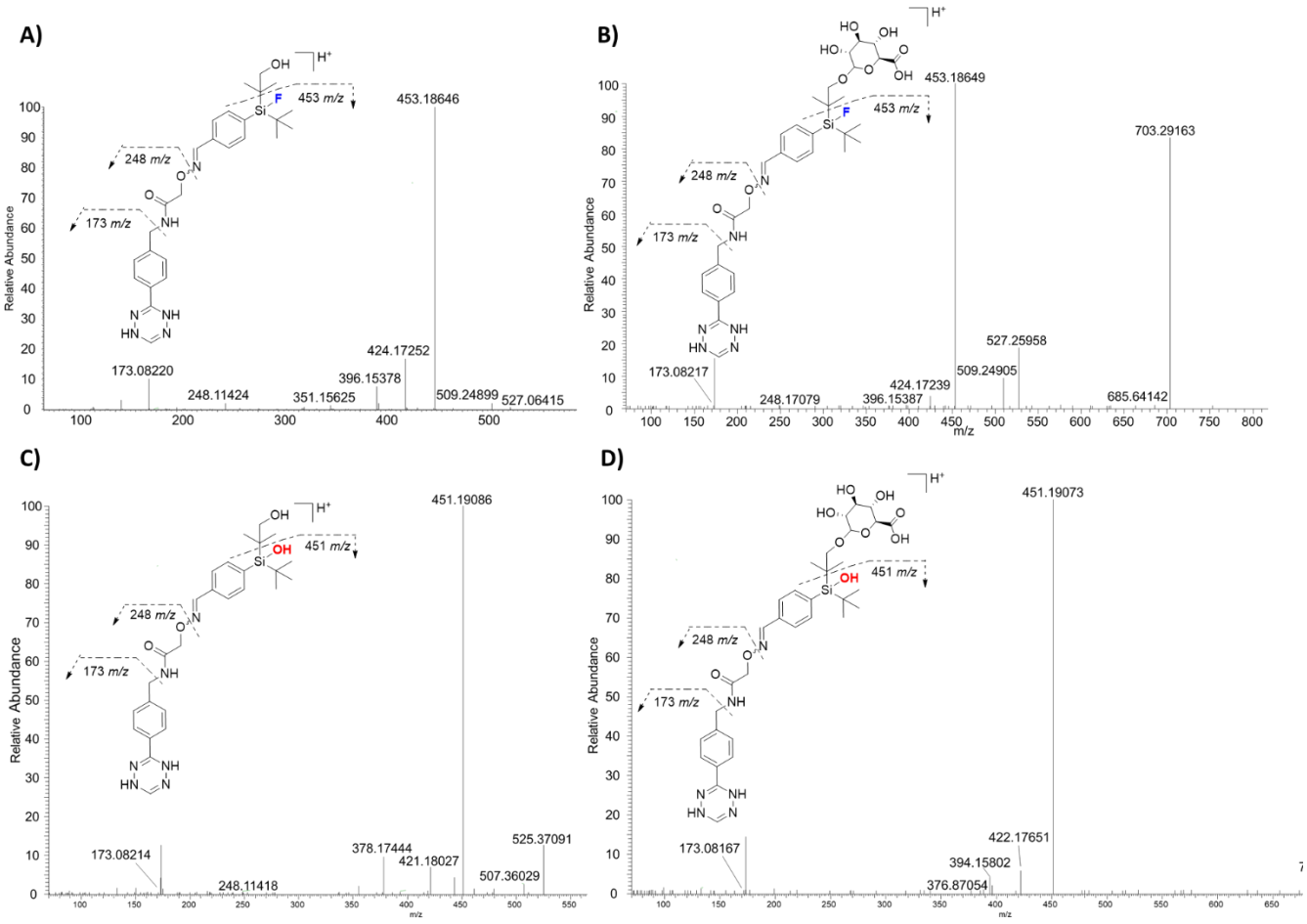

Figure S9. MS^2 -fragmentation patterns for proposed metabolites **M(H$_2$)1**, **M(H$_2$)3 M(H$_2$)5**, and **M(H$_2$)7** of SiFA-H$_2$Tz demonstrating similar fragmentation patterns. (**A**; **M(H$_2$)1** 527.2596 using HCD 20%, **B**; **M(H$_2$)5** 703.2197 using HCD 10%, **C**; **M(H$_2$)3** 525.2640 using HCD 25%, **D**; **M(H$_2$)7** 701.2960 using HCD 20%). Fragments at *m/z* 248 and at *m/z* 173 indicated compound SiFA-H$_2$Tz was subject to no metabolism at tetrazine ring. The *tert*-butyl group adjacent to silicon was apparently hydroxylated and subsequently *o*-glucuronidated. Fragments at *m/z* 507 and at *m/z* 509 from phase I metabolites **M(H$_2$)3** and **M(H$_2$)1** respectively, indicated the cleavage of water (-18 Da). In addition, the cleavage of the glucuronic acid from **M(H$_2$)3** (*m/z* 703) was detected as a fragment with *m/z* 527. The fragments *m/z* 451 from **M(H$_2$)3** and **M(H$_2$)7** and *m/z* 453 from **M(H$_2$)1** and **M(H$_2$)5** were diagnostic fragments verifying the position of *o*-glucuronide at the *tert*-butyl group, by their simultaneous cleavage from the structure.

Fragmentation pattern for proposed metabolite M(H_2)5 (*m/z* 703) using HCD 30%

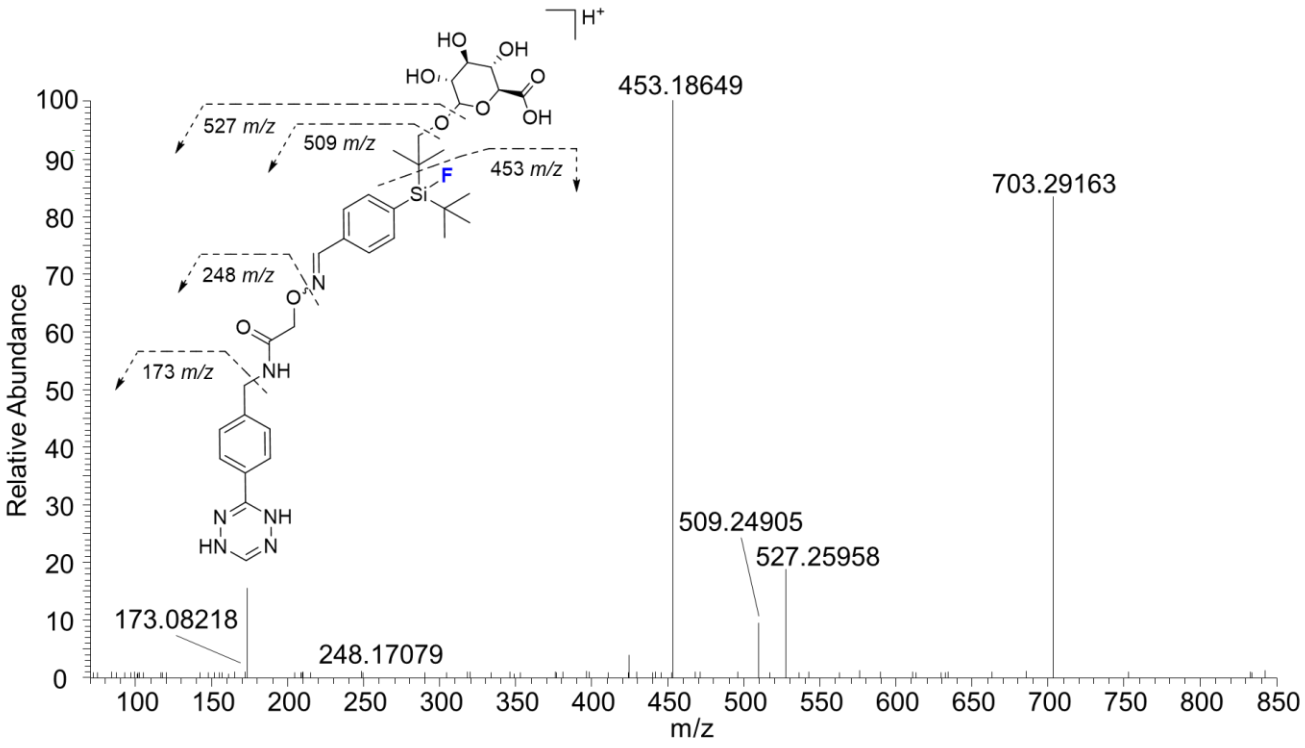

Figure S10. Fragments formed using MS/HRMS for proposed metabolite **M(H_2)5** (*m/z* 703) using HCD 30% of SiFA–H_2Tz demonstrating characteristic fragments at *m/z* 527, *m/z* 509, *m/z* 453, *m/z* 248 and *m/z* 173.

MS/MS/HRMS (MS^3)–spectrum and fragmentation pattern of proposed metabolite M6 of SiFA-Tz.

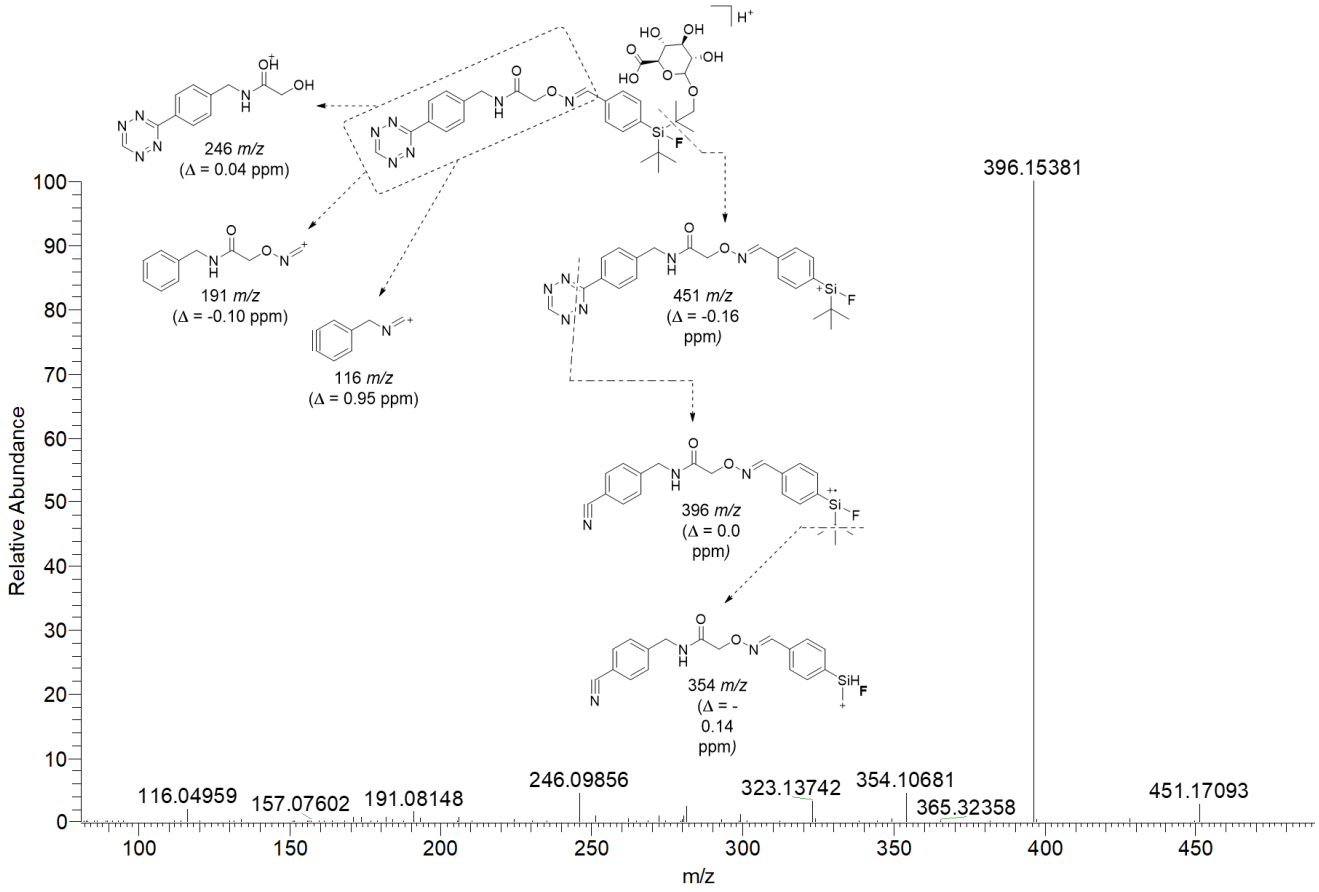

Figure S11. Fragmentation pattern of proposed metabolite **M6** (*m/z* 701.27497, t_R = 3.67 min) at *m/z* 451 using HCD 25% (Δ; mass difference in ppm).

Extracted ion chromatograms of proposed hydroxylated and *o*-glucuronidated metabolites M(H_2)3 and its defluorinated analogue M(H_2)4.

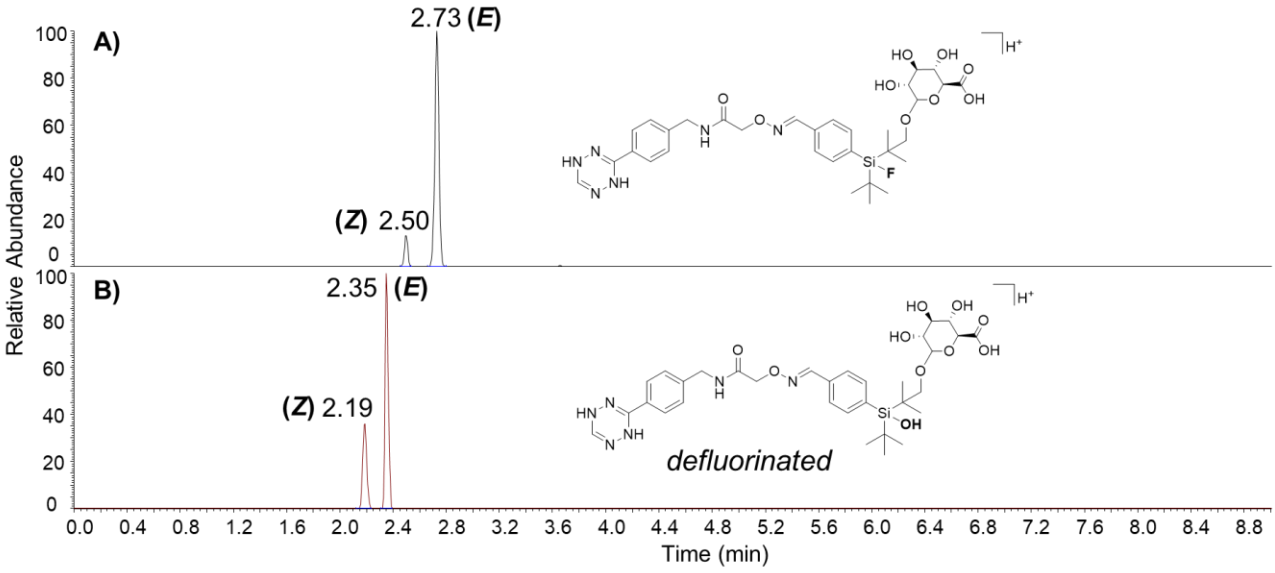

Figure S12. Proposed metabolites of SiFA–H_2Tz. EICs of hydroxylated and *o*-glucuronidated metabolite **A**) **M(H_2)3** (*m/z* 703) and **B**) its defluorinated analogue **M(H_2)4** (*m/z* 701). The difference in the retention time between the two metabolites **M(H_2)3** and **M(H_2)4** is due to the lipophilicity difference of OH and F. Additionally the pairs of peaks indicate presence of analogous (*E*/*Z*)-isomers. Both *E*- and *Z*-isomers (**M(H_2)4** *E*-isomer 85 ± 2%, **M(H_2)3** *E*-isomer 82 ± 1%) were detected in phase II *in vitro* samples.